Title

Regional Brain Shape Abnormalities Persist into Adolescence after Heavy Prenatal Alcohol Exposure

Journal

Cerebral Cortex, 12(8)

ISSN

1047-3211

Authors

Sowell, Elizabeth R
Thompson, Paul M
Mattson, Sarah N
et al.

Publication Date

2002-08-01

DOI

10.1093/cercor/12.8.856

Peer reviewed

Regional Brain Shape Abnormalities Persist into Adolescence after Heavy Prenatal Alcohol Exposure

Elizabeth R. Sowell, Paul M. Thompson, Sarah N. Mattson[1], Kevin D. Tessner, Terry L. Jernigan[2], Edward P. Riley[1] and Arthur W. Toga

Laboratory of Neuro Imaging, Department of Neurology, University of California, Los Angeles, CA, [1]Center for Behavioral Teratology, San Diego State University, San Diego, CA and [2]Department of Veterans Affairs Medical Center and Departments of Psychiatry and Radiology, School of Medicine, University of California, San Diego, CA, USA

We assessed regional brain shape abnormalities and spatial relationships between brain shape and abnormalities observed in the underlying tissue in children and adolescents prenatally exposed to large quantities of alcohol. We used high resolution, 3-D, structural magnetic resonance imaging data and novel, whole-brain, surface-based image analysis procedures to study 21 subjects with heavy prenatal alcohol exposure (8–22 years, mean age 12.6 years) and 21 normally developing control subjects (8–25 years, mean age 13.5 years). Significant brain size and shape abnormalities were observed in the alcohol-exposed subjects in inferior parietal/perisylvian regions bilaterally, where their brains appeared to be narrower than those of the controls in the same general location where they also had increased gray matter density. Highly significant decreased brain surface extent or reduced brain growth was also observed in the ventral aspects of the frontal lobes most prominent in the left hemisphere. For the first time in this report we have mapped brain morphologic abnormalities to the cortical surface in subjects with prenatal alcohol exposure and have shown that the size and shape of the brain is altered in these individuals. The results imply that brain growth continues to be adversely affected long after the prenatal insult of alcohol exposure to the developing brain and the brain regions most implicated, frontal and inferior parietal/perisylvian, may be consistent with behavioral deficits characteristic of individuals prenatally exposed to alcohol.

Introduction

Fetal alcohol syndrome (FAS) describes a constellation of symptoms often found in infants born to alcohol-abusing mothers (Jones and Smith, 1973). These symptoms include prenatal growth deficiency, developmental delay, craniofacial anomalies (i.e. microcephaly, epicanthal folds, short palpebral fissures) and limb defects. Roughly 10–40% of children born to alcohol-abusing mothers meet criteria for the diagnosis (Jones and Smith, 1973; Abel and Sokol, 1987). Brain abnormalities, most commonly microcephaly and neuronal migration anomalies, have been documented in *post mortem* studies (Jones and Smith, 1973; Roebuck *et al.*, 1998). Mental retardation is common among FAS individuals (Abel and Sokol, 1987) and subtler neuropsychological abnormalities have also been reported (Mattson and Riley, 1998). Additionally, behavioral and psychosocial problems are frequently observed in these subjects (Roebuck *et al.*, 1999).

In vivo quantitative magnetic resonance imaging (MRI) studies have confirmed brain morphologic abnormalities in children prenatally exposed to alcohol and have allowed a more detailed account of some of the subtler structural dysmorphology previously observed in these subjects in *post mortem* studies. Recently, we have applied whole-brain MR image analysis techniques to a group of children, adolescents and young adults with prenatal alcohol exposure. The first of these studies (Archibald *et al.*, 2001) utilized volumetric methods and showed that within the cortex, only the parietal lobes were significantly reduced in volume above and beyond the generalized microcephaly observed in these subjects. It also showed that white matter hypoplasia was more significant than gray matter hypoplasia and relative sparing of hippocampal volume was noted. Other research groups have also used quantitative methods to document generalized microcephaly (Swayze *et al.*, 1997). In another study by our group of the same prenatally alcohol-exposed (ALC) subjects, voxel-based morphological analyses were conducted where brain tissue abnormalities in the whole brain were analyzed at once on a voxel-by-voxel basis. Results from this study (Sowell *et al.*, 2001b) complemented findings from the volumetric studies, revealing abnormalities most prominently in the perisylvian cortices of the temporal and parietal lobes where the ALC subjects tended to have increased gray matter density and decreased white matter density. These findings are also consistent with what would be expected given our studies of corpus callosum morphology in ALC subjects, which show that the regions of the corpus callosum that connect perisylvian cortices between the two hemispheres are the most severely affected (Sowell *et al.*, 2001a). Quantitative methods were also used by another research group to document callosal shape abnormalities in FAS (Bookstein *et al.*, 2001).

While volumetric and voxel-based image analyses have tended to localize cortical tissue abnormalities to parietal lobe regions, little is known about abnormalities on the overlying cortical surface of the brain. The purpose of the present study was to analyze brain surface shape abnormalities in a group of children, adolescents and young adults with prenatal alcohol exposure and to assess relationships between cortical gray matter density on the brain surface and brain shape. In the present report, we carefully match brain surface anatomy across individuals by defining cortical sulcal landmarks that can be identified on the brain surface of every individual, thereby ensuring accurate localization of group differences relative to sulcal landmarks. Understanding spatial and temporal relationships between brain shape on the one hand, and tissue density changes on the other hand, could help shed light on the biological processes contributing most to the brain dysmorphology in these individuals observed in earlier structural MRI studies. Additionally, understanding the relationships between regional and temporal patterns of abnormal brain shape and cortical tissue density abnormalities could provide further insight into patterns of cognitive and behavioral deficits characteristic of FAS. Analyzing brain shape in these surface-based analyses allows us to assess regional abnormalities in brain volume, independent of the tissues that comprise the brain in any given region and without the limitations of volumetric studies where regional boundaries must be identified. Using these methods, we predicted that we would see shape abnormalities in the perisylvian and inferior parietal regions, the same regions where we observed increased cortical gray matter density in these subjects in an earlier report

(Sowell *et al.*, 2001b). While we have not seen evidence for frontal lobe abnormalities in the volumetric (Archibald *et al.*, 2001) or voxel-based (Sowell *et al.*, 2001b) analyses of these subjects, we predicted here that we would observe frontal lobe anomalies that might not be reflected in the volumes or tissue density of these regions. This hypothesis was based on the cognitive and behavioral literature which suggests that children with prenatal alcohol exposure have difficulties with response inhibition, behavioral control and executive functions (Olson *et al.*, 1998; Mattson *et al.*, 1999), all known to be related to frontal lobe functioning.

Materials and Methods

Subjects

Twenty-one children, adolescents and young adults with prenatal alcohol exposure who were between the ages of 8 and 22 years (mean age 13 years, 11 female, two left handed) were studied with MRI and surface-based image analyses. All of the children and young adults had histories of behavioral problems, cognitive impairment and heavy prenatal alcohol exposure. Fourteen of them had the characteristic facial appearance – i.e. short palpebral fissures, epicanthal folds, maxillary hypoplasia (Jones and Smith, 1975) – that allowed for a diagnosis of FAS (mean age 12.6 years, eight female, one left handed). Seven other subjects did not have the facial features to warrant a diagnosis of FAS and are instead referred to as subjects with prenatal exposure to alcohol (PEA; mean age 13 years, three female, one left handed). Both alcohol-exposed groups were evaluated by Kenneth Lyons Jones MD, a pediatric dysmorphologist at the University of California, San Diego (UCSD). Children in the alcohol-exposed groups were referred by Dr Jones, other professionals, or were self-referred by parents. Children in the FAS and PEA groups were born to women known to drink heavily during pregnancy, in either a binge fashion or more regularly. As in most retrospective studies involving FAS and prenatal alcohol exposure, exact amounts and patterns of maternal drinking were typically not available. All children were screened for prenatal exposure through caregiver self-report. Additionally, for children in the alcohol-exposed groups, maternal self-report, medical, social and/or legal records were reviewed to confirm prenatal alcohol exposure and to rule out heavy use of other drugs. Both alcohol-exposed groups exhibited neuropsychological deficits relative to the controls, but did not differ significantly from each other. Details of these data are presented elsewhere (Mattson *et al.*, 1996, 1999; Mattson and Riley, 1999), but full-scale IQ scores are similar for both alcohol-exposed groups (FAS mean = 77, SD = 15, range 49–92; PEA mean = 86, SD = 14, range 64–101). The FAS and PEA groups (i.e. ALC) were combined for the statistical analyses to increase power, given that similar results have been observed for PEA and FAS subjects in earlier studies of brain morphology (Archibald *et al.*, 2001; Sowell *et al.*, 2001a,b).

Twenty-one normal children, adolescents and young adults between 8 and 25 years of age were studied as a comparison group (mean age 13.5, 12 female, all right handed) in the surface-based brain image analyses. All child and adolescent subjects were recruited as normal controls for a large, multidisciplinary neurodevelopmental research center or for the Center for Behavioral Teratology, both in San Diego. Each subject was screened for neurological impairments and for any history of learning disability or developmental delay. Informed consent was obtained from all children and their parents. The young adult subjects were recruited as normal controls for neuropsychiatric studies of adult patient populations. These subjects were thoroughly screened for medical, neurological and psychiatric disorders, and again informed consent was obtained from each subject.

The subjects studied here (ALC and control subjects) are the same subjects examined in our earlier reports of callosal (Sowell *et al.*, 2001a) and tissue density abnormalities (Sowell *et al.*, 2001b). These subjects (ALC subjects and controls) also comprise a subset of a larger group studied earlier with volumetric methods (Archibald *et al.*, 2001). Seventeen ALC subjects (10 FAS, seven PEA) and 19 controls were studied with both surface-based methods conducted at the UCLA Laboratory of Neuro Imaging and with volumetric methods conducted at the UCSD Brain Image Analysis Laboratory (Archibald *et al.*, 2001).

Imaging Protocol

Three whole-brain image series were collected for each subject at one of two locations: either UCSD/AMI Magnetic Resonance Institute or Scripps Clinic and Research Foundation. Both locations utilize a 1.5 T superconducting magnet (Signa; General Electric, Milwaukee, WI) and the same image acquisition protocol. The first image series, used for all surface-based and some *post hoc* volumetric image analyses, was a gradient-echo (SPGR) T_1-weighted sagittally acquired series with T_R = 24 ms, T_E = 5 ms, NEX = 2, flip angle = 45°, field of view = 24 cm, section thickness = 1.2 mm (0.9375 × 0.9375 mm within-plane), no gaps (Fig. 1). The second and third series, used for volumetric analyses, were fast spin-echo (FSE) acquisitions yielding two separate coronally acquired image sets: T_R = 3000 ms, T_E = 17 ms, ET = 4; and T_R = 3800 ms, T_E = 102 ms, ET = 8. For all series, the field of view was 24 cm. Section thickness for the FSE series was 4 mm, no gaps (interleaved). Imaging time for all series totaled ~30 min.

Image Processing for Surface-based Analyses

The SPGR MR images from each individual were processed with a series of manual and automated procedures, which are described in detail in other reports (Sowell *et al.*, 1999; Thompson *et al.*, 2001) and summarized here.

Preprocessing

First, each image volume was roughly resliced into a standard orientation by trained operators who 'tagged' 10 standardized anatomical landmarks in each subject's image data set that corresponded to the same 10 anatomical landmarks defined on the ICBM-305 average brain (Mazziotta *et al.*, 1995). Next, brain image volumes were more carefully spatially registered to each other by defining 80 standardized, manually defined anatomical landmarks (40 in each hemisphere, the first and last points on each of 20 sulcal lines drawn in each hemisphere described below) in every individual and using a least-squares, rigid-body transformation to match each individual to the average of all individuals in the data set. In this way, every individual's brain was matched in space, but global differences in brain size and shape remained intact. Semi-automated tissue segmentation was conducted for each volume data set to classify voxels based on signal value as most representative of gray matter, white matter, or CSF (Fig. 1). A simple minimum distance classifier was used because it had previously been shown to provide the best results (for this T_1-weighted imaging protocol) in a qualitative comparison of different tissue segmentation algorithms. A detailed discussion of the reliability and validity of the tissue segmentation protocol has been published elsewhere (Sowell *et al.*, 1999). Non-brain tissue (i.e. scalp, orbits) and cerebellar structures were removed from the spatially transformed, tissue-segmented images. Then, each individual's cortical surface was extracted and three-dimensionally rendered using automated software (MacDonald *et al.*, 1994). This software creates a mesh-like surface which is continuously deformed to fit a cortical surface tissue threshold intensity value from the brain volume. The intensity threshold was defined as the MRI signal value which best differentiates cortical CSF on the outer surface of the brain from the underlying cortical gray matter. Each resulting cortical surface was represented as a high-resolution mesh of 131 072 surface triangles spanning 65 536 surface points. Shown in Figure 1 is a sample surface rendering which has been shaded and color-coded to aid in appreciation of the 3-D representation of the cortex.

Anatomical Analysis

Image analysts (K.D.T. and E.R.S.) who were blind to subject diagnosis, sex and age, digitized 3-D models representative of 17 sulci [Sylvian fissure, central, pre-central, post-central, superior temporal sulcus (STS) main body, STS ascending branch, STS posterior branch, primary intermediate sulcus, secondary intermediate sulcus, inferior temporal, superior frontal, inferior frontal, intraparietal, transverse occipital, olfactory, occipito-temporal and collateral sulci] in each hemisphere on the surface rendering of each subject's brain (Fig. 1). In addition to contouring the major sulci that could be identified in every individual, a set of six midline landmark curves bordering the longitudinal fissure were outlined in each hemisphere to establish hemispheric gyral limits. Spatially registered gray-scale image volumes in coronal, axial and sagittal

Figure 1

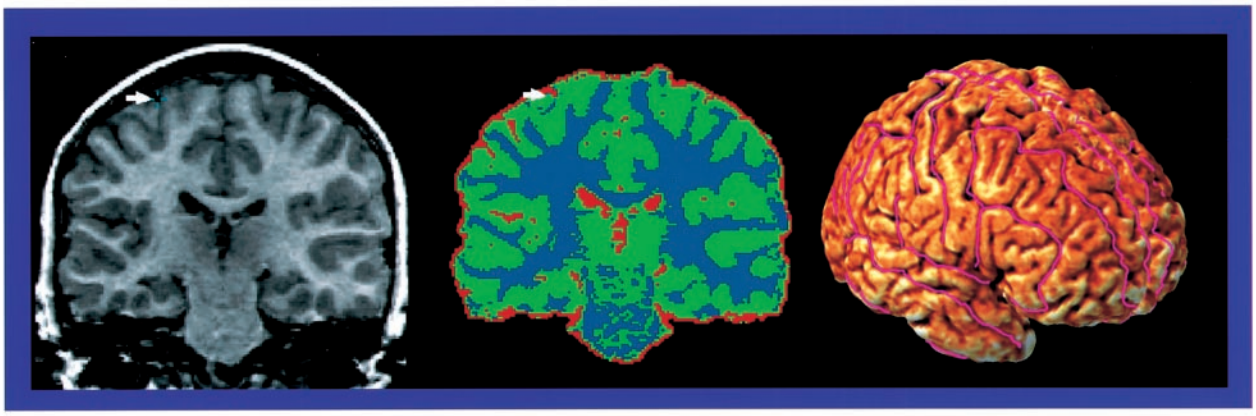

Figure 2

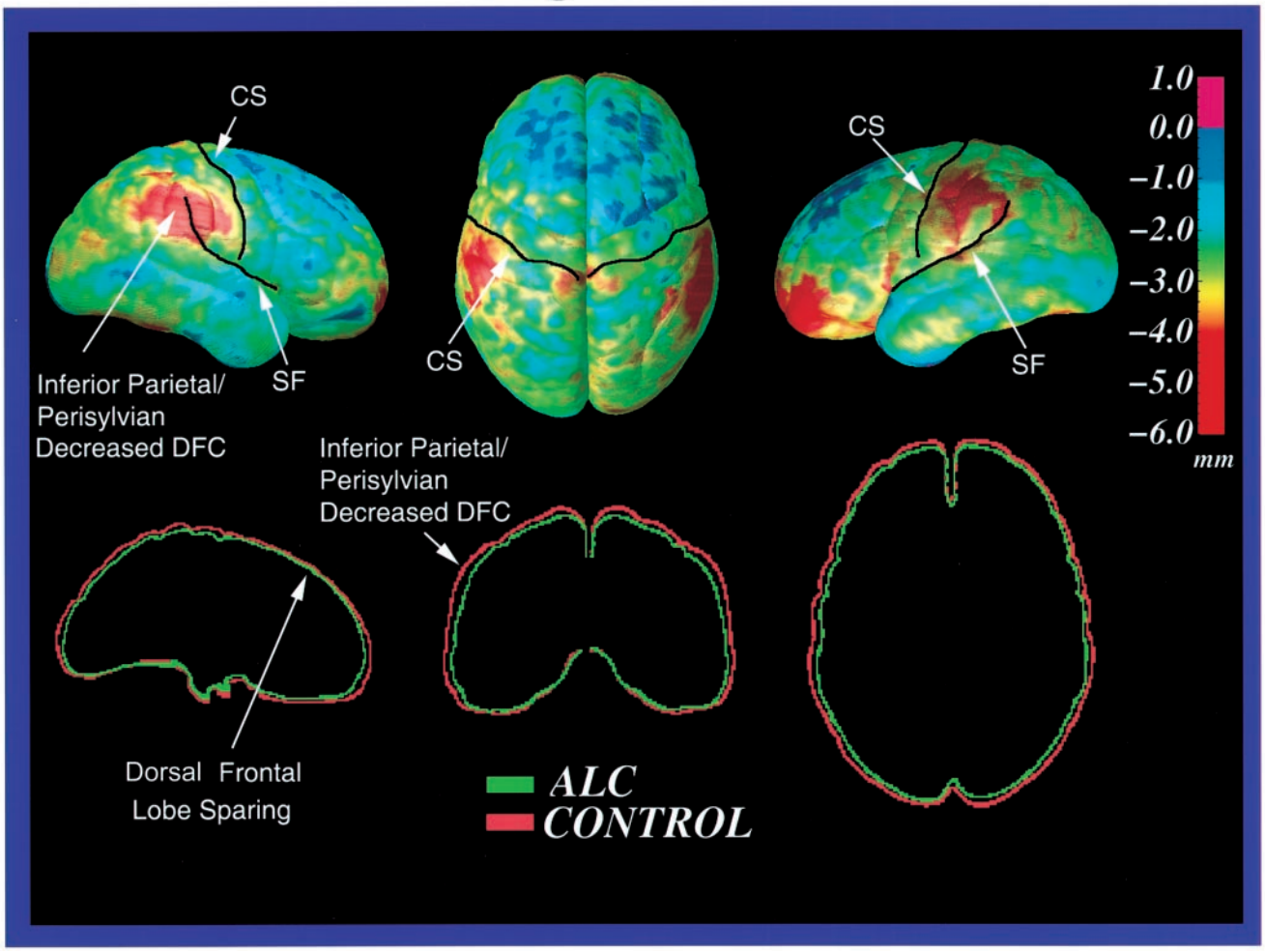

Figure 1. Image analysis procedures. Sample coronal slices through the original T_1-weighted (left) and skull stripped tissue segmented (middle) images, and a sample surface rendering (right) with contours for 17 sulcal landmarks and six midline contours in each hemisphere shown in pink (right frontal view). White arrows highlight crosshairs that represent matching anatomical locations in the two brain slices.

Figure 2. Brain surface extent maps. In the top row are DFC group-difference maps showing differences in DFC (in mm) between the ALC and control subjects according to the color bar on the right. Notice the negative effects in nearly all regions, meaning DFC is greater in the controls than the ALC subjects, with regional patterns of DFC reduction up to 6 mm. In the bottom row are the outlines or edges of the average ALC surface (in green) and the average control surface (in red) in three orthogonal slices (sagittal, coronal and axial). Note the close correspondence of the edges (relative sparing) near the dorsal frontal surface of the brain and the large disparities over the dorsal convexity, particularly in the parietal/perisylvian region.

planes were available simultaneously to help disambiguate brain anatomy. We have developed detailed criteria for delineating the cortical lines, and for starting and stopping points for each sulcus, using brain surface atlases as references (Ono *et al.*, 1990; Duvernoy *et al.*, 1991). These criteria, along with interrater reliability measures, have been described previously (Sowell *et al.*, 2002a) and complete details of the written anatomical protocol can be obtained from the authors.

Gray Matter Density and Surface Shape Measures

Points on the cortical surfaces surrounding and between the sulcal contours drawn on each individual's brain surface were calculated using the averaged sulcal contours as anchors to drive 3-D cortical surface mesh models from each subject into correspondence (Thompson *et al.*, 2000, 2001). This allows the creation of average 3-D surface models for the ALC and control groups, and the creation of group average maps of various features of the brain surface, such as local brain growth or brain shape and gray matter density. In this averaging process, a cortical model with the average shape for the group is generated and features from corresponding gyri are averaged together. The 'distance from the center' or DFC measure has been developed primarily to quantify group differences in local growth or brain shape. It is a measure of radial expansion measured from the center of the brain, roughly at the midline decussation of the anterior commissure (i.e. $x = 0$, $y = 0$, $z = 0$), to each of the 65 536 brain surface points. Note that the distance measure at each point for each individual is reflective of anatomical location in addition to radial expansion, thus only relative differences in DFC are meaningful in terms of brain shape. Because previous reports have shown microcephaly in these subjects (Archibald *et al.*, 2001; Sowell *et al.*, 2001b), we also wished to look at local brain shape differences which were independent of global differences in head size. Thus, we conducted exploratory analyses of DFC in which the brain data sets were transformed into a standard orientation — ICBM-305 space (Mazziotta *et al.*, 1995) — using an automated, 12 parameter, linear transformation (with scaling) (Woods *et al.*, 1993) resulting in new brain size corrected image data sets for each individual. Because the scaling into ICBM 305 space was linear, brain shape was generally preserved and all images and anatomical delineations were easily, automatically transformed between the resliced (without scaling) and the scaled ICBM 305 spaces.

Because the deformation maps (acquired during cortical surface matching) associate the same cortical anatomy in each subject (based on sulcal contours drawn in each individual), a local measurement of gray matter density (at each point over the surface of the brain) could be made for each subject in addition to the DFC measures and averaged across corresponding regions of cortex (Thompson *et al.*, 2001; Sowell *et al.*, 2002a). Briefly, a sphere with a radius of 15 mm centered at each cortical surface point was made and referenced to the same spatial location in the gray matter maps for each subject derived earlier in the tissue classification. The proportion of segmented gray matter voxels relative to the total number of voxels in this sphere was computed (at each point) and stored as a map of gray matter proportion (with values 0.0–1.0), for each subject. The proportion of gray matter in each sphere in each individual is reflective, in part, of local cortical thickness that varies over different regions of the brain.

Image Processing for Volumetric Analyses

Detailed descriptions of the volumetric image-analytic approach used in the UCSD Brain Image Analysis Laboratory are provided in the previous report of volumetric results in the larger group of ALC subjects (Archibald *et al.*, 2001) and in other reports (Jernigan *et al.*, 2001; Sowell *et al.*, 2002b). While many regions of interest are defined for each subject as part of the standard image analysis protocol at UCSD, here we were interested in volumetric measures best corresponding to our analyses of brain shape and tissue density at the cortical surface. Thus, measures studied here included total volume (including gray matter, white matter and CSF), gray matter volume, white matter volume and CSF volume in the frontal, temporal, parietal and occipital lobes. Again, given that brain size is reduced in the ALC subjects, we also assessed effects of group membership on total lobar volumetric measures (including gray matter, white matter and CSF) that were not attributable to group differences in total supratentorial cranial volume. In these analyses, new proportional measures were created where each lobar volume measure was entered as the numerator and total supratentorial cranial volume was entered as the denominator.

Statistical Analyses for Surface-based Measures

After the basic preprocessing steps were conducted for each individual, statistical maps of differences between groups were created for gray matter density and DFC. In these analyses, the correlation (Pearson's r) between group membership and (1) gray matter density or (2) DFC at each brain surface point was calculated. For the gray matter group difference statistical maps, a surface point threshold of $P = 0.01$ was used. A more stringent surface point threshold, $P = 0.001$, was used for the DFC analysis, given that earlier reports have shown global microcephaly in the ALC subjects studied here (Archibald *et al.*, 2001). Consequently, we expected relatively large decreases in DFC overall, but were interested in looking at localized patterns of group differences over the brain surface. Permutation tests were conducted to assess the significance of the statistical maps (gray matter and DFC) and to correct for multiple comparisons. Anatomical regions of interest (ROI) were used in the permutation analyses to test our *a priori* hypotheses for DFC that we would see abnormalities in perisylvian and frontal regions. Gross frontal lobe, parietal lobe, temporal lobe and occipital lobe ROIs were created for each individual from a probabilistic atlas (Evans *et al.*, 1996) by transforming the probabilistic ROIs from standardized space back into the resliced space of each individual using an automated 12 parameter affine transformation (Woods *et al.*, 1993). The new ROIs for all individuals were then averaged to create regional masks, reducing the search area to specific brain regions in the permutation analyses. The number of surface points within each ROI that was significant at a threshold of $P = 0.001$ (for the DFC analyses) was compared to the number of significant surface points within the ROI that occurred by chance when subjects were randomly assigned to groups in 10 000 new analyses. Negative (control > ALC) and positive (ALC > control) effects were assessed separately. Again, this allowed us to determine the null distribution to assess the overall statistical significance of our results within the four ROIs. The same ROIs were used for the gray matter maps, but a threshold of $P = 0.01$ was used.

Statistical Analyses for Volumetric Measures

Statistical analyses for the volumetric data in 17 of the ALC subjects and 19 of the controls were conducted to cross-validate results from surface-based and volumetric analyses in the same subjects, and to confirm results reported earlier (Archibald *et al.*, 2001) in the smaller sample studied here. Spearman correlation coefficients (i.e. rho) were calculated to assess the relationship between group membership and the volume measures for frontal, parietal, temporal and occipital lobes (total lobar volume, and gray matter, white matter and CSF volume within each lobe). We also assessed group effects for the proportional lobar volume measures. The Spearman correlation coefficient is similar to the Pearson correlation coefficient, but was used because it is relatively robust to the effects of leverage and outliers that can occur with these volumetric data.

Image and Statistical Analyses for Post Hoc Volumetric Measures

Finally, *post hoc* volumetric analyses were conducted in order to assess relationships between group differences in volume measures of temporal lobe gray matter and group differences in temporal lobe gray matter density from the surface-based analyses. These analyses are critical to assess the validity of the statistical maps where image averaging was used. Two new temporal lobe ROIs (in each hemisphere) were automatically defined in the high-resolution T_1-weighted image data sets for each individual, based on the statistical maps of gray matter density increase in ALC subjects and a probabilistically defined temporal lobe region (Evans *et al.*, 1994). The first ROI was created by selecting all surface points where the group difference in gray matter density (increased gray matter density in ALC subjects) was significant at a probability of 0.001 or less. The single-voxel layer of surface points (since we only measured statistics at the cortical surface) that were significant at $P = 0.001$ or less were then dilated with a 15 mm radius (to emulate the 15 mm radius sphere in the surface-based gray matter density analyses), resulting in a group average statistical ROI encompassing all voxels which showed a statistically significant increase in gray matter density and were within a 15 mm radius of the brain surface. Next we subtracted all voxels from the

statistical ROI that did not fall within the probabilistically defined average temporal lobe region and called the resulting ROI the 'temporal lobe statistical ROI'. The second ROI encompassed all voxels that fell within the probabilistically defined temporal lobe but not within the statistical ROI. We refer to this ROI as the 'non-statistical temporal lobe ROI'. Finally, we automatically transformed the ROIs in group average space into the non-scaled image space of each individual subject and counted all voxels that segmented as gray matter and fell within each ROI for each individual to obtain volume measures. Note that these *post hoc* volumetric analyses were carried out on the high-resolution T_1-weighted series for all 42 subjects rather than relying on the anatomical ROIs defined on the lower-resolution data sets for fewer subjects. Correlational analyses (using Spearman's rho) were conducted to assess group effects for the volumes of gray matter within the temporal lobe statistical ROI and the non-statistical temporal lobe ROI.

Results

Brain Size/Shape Differences

Group effects (ALC minus controls) are shown where the difference in brain surface extent or local brain growth (i.e. DFC) in millimeters between the ALC subjects and controls is illustrated according to the color scale (Fig. 2). Note first that the average brain surface extent is smaller in the ALC subjects in most locations, as would be expected given their microcephaly. Prominent regional patterns emerge, however, when size and shape differences are considered on a point-by-point basis over the entire brain surface. DFC in inferior parietal/perisylvian regions bilaterally is dramatically reduced by ~4–6 mm in the ALC subjects relative to controls. The anterior and orbital frontal cortex, particularly in the left hemisphere is also considerably reduced in the ALC subjects. These are regions where the cortical surface is closer to the center of the brain in the ALC subjects, perhaps where there has been less local brain growth. The dorsal frontal cortex appears least affected, with only ~0–1 mm difference between groups. These effects are also shown in the lower portion of Figure 2, which highlights the shape as well as the size differences between the ALC and control subjects. A statistical map of DFC differences shows that the relatively large group differences in bilateral inferior parietal/perisylvian cortices and in the left orbitofrontal cortex are statistically significant (Fig. 3). ROI permutation tests presented in Table 1 confirm the significance of DFC decreases (while correcting for multiple comparisons) in the ALC group in parietal, temporal and frontal lobes.

Gray Matter Density

A statistical map of differences in gray matter density between the ALC and control subjects is shown (Fig. 4). Note the large regions in the inferior parietal and perisylvian cortex bilaterally (more prominently in the left hemisphere) where the gray matter density is increased in the ALC subjects relative to control subjects. This result was expected given our earlier findings (Sowell *et al.*, 2001b). However, in the present report, gray matter density at homologous anatomical surface points was ensured, given that each subject's anatomy was matched on surface sulci rather than relying on the automated methods for anatomical matching used in the previous report. The ALC subjects have an estimated 15% more segmented gray matter in the regions where group differences are significant. Note that the highly significant gray matter density increases measured here are also likely reflective of reductions in white matter in the perisylvian regions, given that less gray matter tissue at each surface point means that more white matter or CSF is present. Permutation analyses within lobar ROIs confirmed the significance of the tissue abnormality spanning across the perisylvian cortices of the parietal lobes bilaterally and the temporal lobes, particularly in the left hemisphere, as shown in Table 1.

Table 1
Surface permutation results: group effects for ROI permutation analyses for gray matter and DFC where the *P*-values presented reflect the proportion of random tests (out of 10 000) in which the number of significant surface points exceed the number of significant surface points observed in the real test

Lobar region	Gray matter ($P = 0.01$)				DFC ($P = 0.001$)			
	Positive *P*-value		Negative *P*-value		Positive *P*-value		Negative *P*-value	
	L	R	L	R	L	R	L	R
Frontal	0.0357	0.0148	0.2658	0.4112	1.000	1.000	0.0006	0.0036
Parietal	0.0002	0.0009	0.4873	0.5601	1.000	1.000	0.0009	0.0002
Temporal	0.0004	0.0037	0.4309	0.2214	1.000	1.000	0.0014	0.0030
Occipital	0.0232	1.000	0.1343	0.0311	1.000	1.000	0.0235	0.0048

Results are tabulated by hemisphere. Negative effects mean that ALC subjects have smaller values on the measure and positive effects mean that the ALC subjects have larger values on the measure. Results that are greater than $P = 0.003$ are not considered significant once a Bonferroni correction (to protect against type 1 error at $P = 0.05$) is applied for the 16 tests for each measure (i.e. left and right hemisphere for each of four lobes).

Note that our *a priori* hypotheses are supported with these data, given that decreased DFC is observed in the inferior parietal region overlapping with regions where we see an increase in gray matter density in the ALC subjects (Fig. 5).

In order to investigate regional brain shape abnormalities that were independent of the overall microcephaly, we created DFC statistical maps in scaled standard image space – International Consortium for Brain Mapping average 305 space (Mazziotta *et al.*, 1995) – where each subject's brain image data were linearly transformed to remove brain size differences while conserving basic brain shape (Fig. 6). Note the relatively large regions of decreased DFC in the ALC subjects in the inferior parietal and perisylvian region bilaterally, strikingly similar to the same effects observed in non-scaled space (Fig. 6). These results confirm that the brain shape abnormality in the inferior parietal cortex is above and beyond that which would be expected from the more global microcephaly in these subjects. Interestingly, new results are observed in dorsal frontal cortex, where the ALC subjects have increased DFC relative to the controls once brain size differences are linearly scaled. Note that these effects are at trend-level significance for increase in DFC in the frontal lobes when gross lobar ROIs (Evans *et al.*, 1996) are used in permutation analyses (left frontal, $P = 0.081$; right frontal, $P = 0.075$). Also, significant decreases in DFC in the ALC subjects were observed in permutation analyses of the right parietal lobe ROI ($P = 0.019$) and trend-level significant results are observed in the left parietal lobe ROI ($P = 0.091$).

Volumetric Analyses

Results from volumetric analyses of frontal, temporal, parietal and occipital cortical regions are presented in Table 2 and are generally consistent with those reported earlier in the larger sample (Archibald *et al.*, 2001). The parietal lobes appear to be the most affected, though significant volume reductions are observed in the frontal and temporal lobes as well. Highly significant white matter volume reductions are observed in left hemisphere parietal and temporal lobes, perhaps consistent with the highly significant gray matter density increase (or white matter density reduction) in these regions observed in the surface-based analyses. Gray matter volume reduction is significant only in the parietal lobe, though based on the spatial

Figure 3

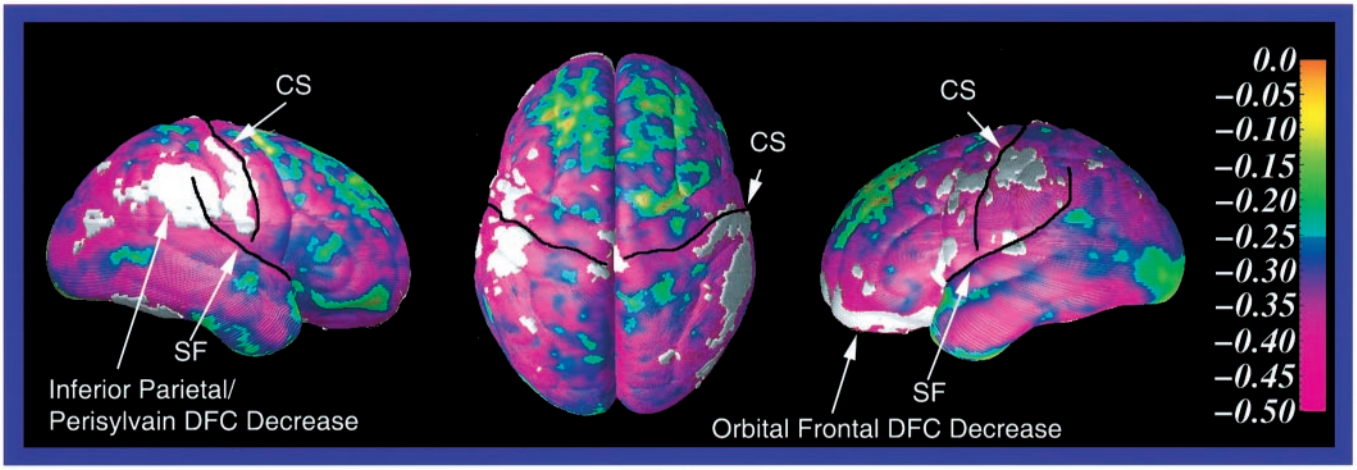

Figure 4

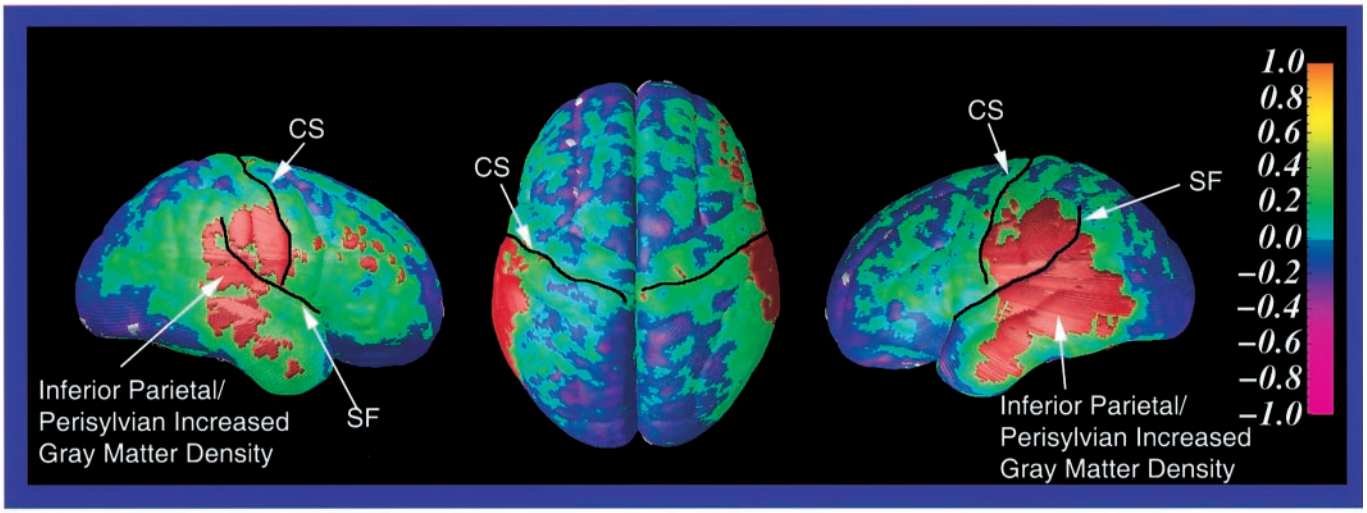

Figure 3. Brain surface extent statistical maps. DFC group-difference statistical maps showing differences in DFC between the ALC and control subjects in resliced (non-scaled) space according to the color bar on the right (range of Pearson correlation coefficients from –1 to +1). As shown, most regions have negative Pearson's correlation coefficients (decreased DFC in ALC subjects relative to controls). Regions overlaid in white correspond to correlation coefficients that show significant decrease in DFC in ALC subjects at a threshold of $P = 0.001$. Positive correlations (i.e. increased DFC in ALC subjects relative to controls) were not significant at this threshold in any region. The Sylvian fissure (SF) and central sulcus (CS) are highlighted for anatomical reference.

Figure 4. Gray matter density statistical maps. Gray matter density group-difference statistical maps showing gray matter density increase (and white matter density decrease) in the ALC subjects relative to controls (in non-scaled space). Shades of green to yellow represent positive Pearson's correlation coefficients (increased gray matter density in ALC subjects) and shades of purple and pink represent negative Pearson's correlation coefficients (decreased gray matter density in ALC subjects) according to the color bar on the right (range of Pearson correlation coefficients from –1 to +1). Regions shown in red correspond to correlation coefficients that show significant increase in gray matter in the ALC subjects relative to controls at a threshold of $P = 0.01$. Regions shown in white correspond to correlation coefficients that show significant decrease in gray matter in the ALC subjects relative to controls at a threshold of $P = 0.01$. The Sylvian fissure (SF) and central sulcus (CS) are highlighted for anatomical reference.

maps of gray matter density, it is likely that this effect is carried by local effects in more dorsal regions rather than the more inferior parietal regions where gray matter density increase is observed. As shown in Table 2, all regions are reduced in volume in the ALC subjects, which is consistent with the microcephaly reported previously (Archibald *et al.*, 2001). When lobar volumes were assessed as proportions to total intracranial volume, only the parietal region remained significantly reduced in the ALC relative to controls (rho = –0.36, $P = 0.04$) above and beyond the generalized microcephaly in these subjects. The frontal lobes were actually increased in proportional volume in the ALC subjects at trend-level significance (rho = 0.33, $P = 0.05$). Together, these results may be consistent with the surface-based analyses of DFC in scaled image space, where the parietal DFC was decreased and frontal DFC was actually increased in the ALC group.

Figure 5

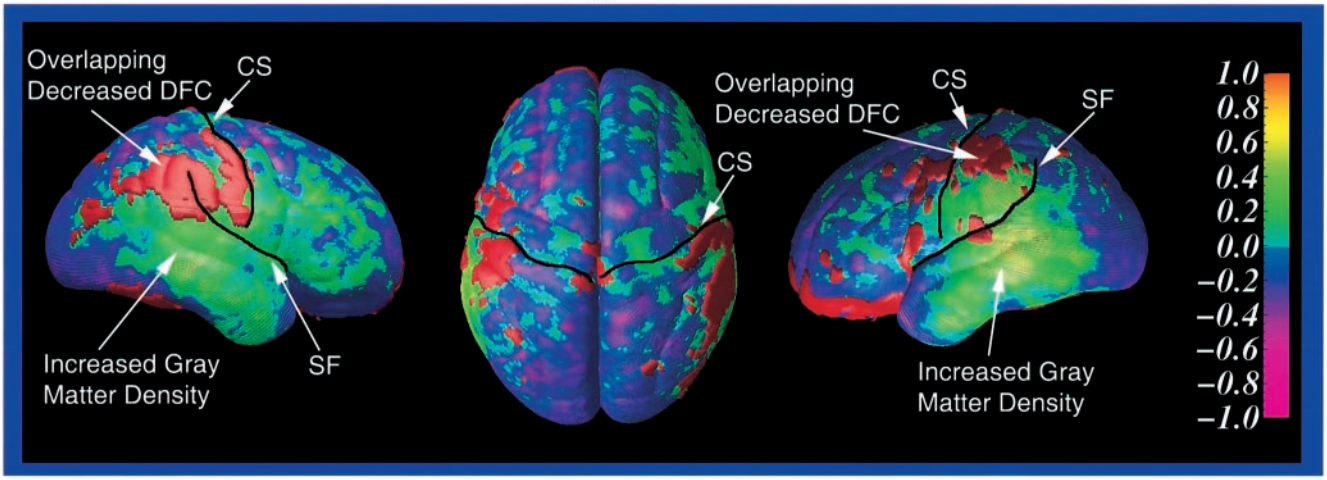

Figure 6

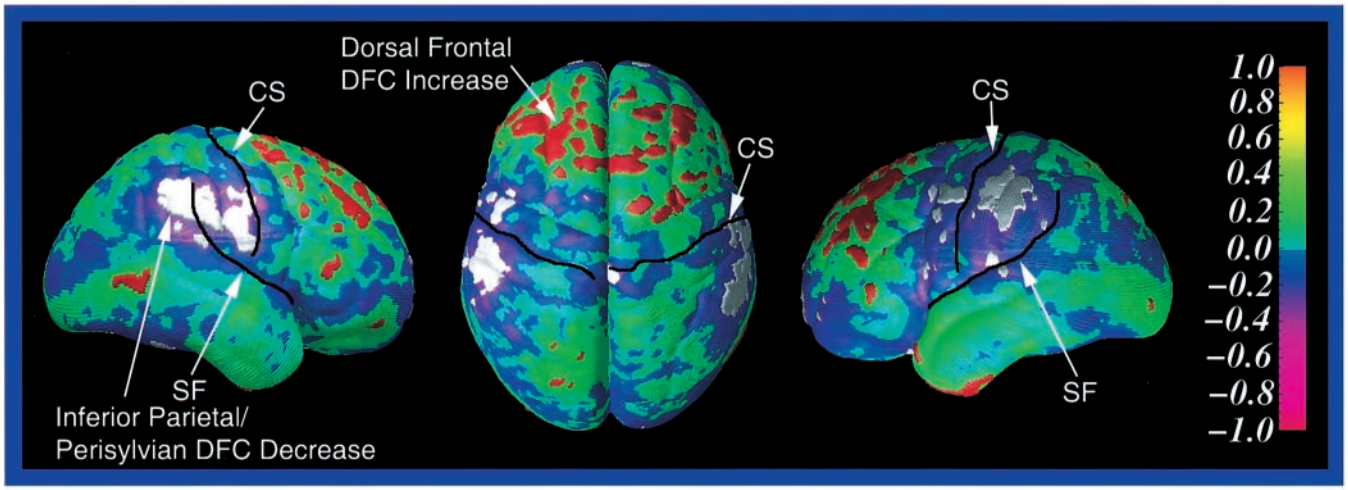

Figure 5. Gray matter versus brain surface extent. Composite statistical maps showing group differences gray matter (Pearson *r* map according to the color bar) with the probability maps for significant differences in DFC ($P = 0.001$) shown overlaid in red (same as shown in white in Fig. 3). Note the highly spatially consistent relationship between gray matter density increase (shown in shades of green and yellow, same as in Fig. 4) and decreased DFC. The shapes of the regions of greatest differences between the groups for the two maps (gray matter and DFC) are very similar in inferior parietal regions, highlighting the regionally inverse relationship between the two features of brain dysmorphology in prenatal alcohol exposure. The Sylvian fissure (SF) and central sulcus (CS) are highlighted for anatomical reference.

Figure 6. Brain surface extent statistical maps in scaled space. DFC group-difference statistical maps showing differences in DFC between the ALC and control subjects in scaled ICBM 305 space. Shades of green to yellow represent positive Pearson's correlation coefficients (increased DFC in ALC patients relative to controls) and shades of purple and pink represent negative Pearson's correlation coefficients (decreased DFC in ALC patients relative to controls) according to the color bar on the right (range of Pearson correlation coefficients from −1 to +1). Regions shown in red correspond to correlation coefficients that show significant increase in DFC in ALC patients at a threshold of $P = 0.05$. Shown in white are regions of significant decreases in DFC in the ALC patients relative to controls at a threshold of $P = 0.05$. Note that lower surface point thresholds were used here given that the large, global brain size effects were removed (with spatial normalization with scaling) leaving only relatively subtle brain shape anomalies observable. The Sylvian fissure (SF) and central sulcus (CS) are highlighted for anatomical reference.

Post Hoc *Volumetric Results*

Gray matter volume reductions in the temporal lobes may seem inconsistent with the large temporal lobe regions of significant increase in gray matter density in the ALC group. However, *post hoc* volumetric analyses of the volume of gray matter in the region directly underlying the region of significant gray matter density increase shown in the surface statistical map show that gray matter volume is actually increased at trend-level significance in the ALC group in this region in the right hemisphere (rho = 0.301, $P = 0.06$) and the remaining temporal lobe cortex is significantly decreased (right hemisphere, rho = –0.327, $P = 0.041$; left hemisphere, rho = –0.488, $P = 0.002$). These results illustrate that within the larger temporal lobe region, there are subregions which are relatively more or less affected in opposite directions and these effects can be detected with surface-based methods.

Table 2

Volumetric results: group effects (Spearman's rho) for total region volumes and regional gray matter, white matter and CSF volumes (in cubic cm)

Brain region	Total region volume(sum of gray, white and CSF)			Regional white matter volume			Regional gray matter volume			Regional CSF volume		
	ALC	CON	Rho (p)	ALC	CON	Rho (p)	ALC	CON	Rho (p)	ALC	CON	Rho (p)
Frontal lobe	40.1	45.5	–0.47 (0.006)	11.47	14.47	–0.55 (0.001)	26.88	29.27	–0.34 (0.044)	1.55	1.47	0.08 (0.62)
Parietal lobe	21.1	25.6	–0.64 (<0.001)	6.49	8.78	–0.65 (<0.001)	13.84	15.92	–0.47 (0.006)	0.45	0.62	–0.07 (0.68)
Temporal lobe	18.3	21.9	–0.56 (0.002)	4.42	6.32	–0.68 (<0.001)	13.42	14.98	–0.35 (0.058)	0.32	0.39	0.00 (0.99)
Occipital lobe	13.9	15.7	–0.34 (0.044)	3.56	4.36	–0.36 (0.032)	10.12	11.10	–0.29 (0.084)	0.14	0.18	–0.01 (0.98)

Results with probabilities that exceeded $P = 0.01$ were not considered significant after a Bonferoni correction (to protect against type 1 errors at $P = 0.05$) was applied for the four statistical tests (one for each lobe) for each tissue type.

Discussion

Results from this study reveal significant brain shape abnormalities in individuals prenatally exposed to alcohol, generally supporting our *a priori* hypotheses. Specifically, robust abnormalities are observed in the lateral perisylvian and parietal regions where the ALC subjects' brains appear to be narrower than the controls. This effect is observed whether the brain size reduction in ALC subjects is taken into account or not, suggesting that the regional shape effect in the perisylvian/inferior parietal region is larger than the overall microcephaly. We also show new findings of decreased brain surface extent in the orbital frontal cortex of alcohol-exposed subjects. Findings of tissue density abnormalities localized primarily to large regions of inferior parietal and superior temporal cortex bilaterally replicate our results from an earlier report (Sowell *et al.*, 2001b) where automated image registration was used. However, by using the novel surface-based methods demonstrated in the present study, we have now been able to localize relatively small regions of gray matter volume increase within the temporal lobes, surrounded by much larger regions of gray matter volume reduction. These effects could not be detected in more traditional volumetric studies, where the temporal lobes were measured as a whole. Finally, here we reveal a spatial distribution of brain surface extent reduction (i.e. decreased DFC) in the ALC subjects that is spatially quite consistent with, but inversely related to the pattern of gray matter density increase. That is, we tend to see regions of increased gray matter density in ALC subjects spatially overlapping with regions of less local growth or lateral extension of the brain.

Recent studies of normal brain development may shed light on maturational processes occurring late in childhood and adolescence, which could lead to the spatial coincidence of gray matter density increase concomitant with decreased surface displacement in the ALC subjects. For instance, inverse relationships between brain growth or surface extent and gray matter density at the brain surface have been shown in normal children and adolescents, such that regions with greater brain growth have less dense gray matter (Sowell *et al.*, 2001c). This is presumably due to relatively late cellular maturational events such as increased myelin (Yakovlev and Lecours, 1967) and reductions in synaptic density (Huttenlocher, 1979), known to occur at these ages. It is important to note that myelin is made of the membranous processes from glial cells that wrap themselves around axons and thus occupies space (Friede, 1989). Our earlier results (Sowell *et al.*, 2001c) suggest that the continued deposition of myelin during late brain development results in a net volume increase and lateral expansion or growth of the brain surface in regions contiguous to the cellular changes. Perhaps the brain is too small and the gray matter appears too dense in the perisylvian and inferior parietal lobes in the ALC subjects because myelin deposition has not occurred normally in these subjects, preventing normal growth and cortical thinning in these regions. Further support for these hypotheses is found in results from animal studies showing that astroglial cells, which are integral in the development of myelin, are particularly affected by alcohol exposure (Guerri, 1998; Guerri *et al.*, 2001). Further, there has been recent interest in prenatal susceptibility of oligodendrocytes to toxicity or injury (Back *et al.*, 1998, 2001). These findings highlight the vulnerability of the myelination process to alcohol exposure, though it should be noted that here we speculate about abnormalities of continued myelination some 7–20 years after the neurotoxic exposure to alcohol. Animal data, however, have shown long-term permanent changes in myelin. For example, postnatal ethanol exposure delivered directly to rat pups over a 6 day period on postnatal days 4–10 reduced the expression of specific myelin basic protein (MBP) and myelin-associated glycoprotein (MAG) isoforms in the cerebellum of animals in adulthood (Zoeller *et al.*, 1994). In this report, we also see regions of increased gray matter density in the absence of brain growth abnormalities (i.e. temporal lobes). This might suggest, alternatively to a lack of myelination, that a lack of normal cortical synaptic pruning had occurred in these regions, resulting in increased gray matter density in the ALC subjects relative to the controls. Longitudinal or animal studies should help further elucidate relationships between regional patterns of cellular changes late in development and resultant brain shape and tissue density abnormalities observed in those with prenatal alcohol exposure.

A discussion of earlier (i.e. during gestation and the first few years of life) cellular events that could lead to the altered brain shape and tissue density abnormalities observed during adolescence in alcohol-exposed subjects is also warranted. Recent hallmark research by Ikonomidou and colleagues shows that perinatal exposure to alcohol in rats during a period coinciding with the sixth month of gestation through 3 years of age in humans leads to widespread neurodegenerative apoptosis in the developing forebrain (Ikonomidou *et al.*, 2000). Ethanol triggers this apoptosis by mediating *N*-methyl-D-aspartate (NMDA) glutamate and $GABA_A$ receptors. Ikonomidou and colleagues also show that vulnerability to apoptotic neurodegeneration is coincident with periods of synaptogenesis (Ikonomidou *et al.*, 2000) and is regionally specific (Ikonomidou *et al.*, 2000, 2001). This could help explain how transient or 'binge' exposures to ethanol during gestation could have large effects on the developing brain and the widespread apoptosis could result in the microcephaly observed in so many individuals with severe prenatal alcohol exposure. Another research group has also reported regional variability in Purkinje and granule cell loss during the first two trimesters equivalent in the rat (Maier and West, 2001), which may help explain why we observe

regional variability in decreased brain size and tissue density abnormalities in the population studied here.

Relationships between gray matter density and DFC may also be due to differences in brain surface curvature in different brain regions. Arguably, a sphere centered on a more curved surface would have less gray matter within it than a sphere centered at the same anatomical point on a flatter surface, even if the gray matter within the spheres had the same thickness. Perhaps the ALC subjects have more gray matter in perisylvian regions because their brain surfaces are less curved in these regions. However, the regions of most significant gray matter density increase fall just inferior to regions of greatest group difference in DFC, where the average ALC brain surface does appear to be less convex. We are actively pursuing automated methods for measuring cortical thickness without the confounding factors of surface curvature and sulcal depth, as are other research groups (MacDonald *et al.*, 2000; Miller *et al.*, 2000).

The abnormalities observed in the dorsal frontal cortex in the surface-based analyses are also consistent with our *a priori* hypotheses, though the results in this region are more difficult to interpret. Diffuse reductions in dorsal frontal lobe DFC are observed in the ALC subjects when brain size correction is not used and local increases in DFC are observed when brain size correction is used. This could indicate that shape abnormalities in the dorsal frontal lobes are more prominent than size reductions. However, while the algorithm (Woods *et al.*, 1993) used to scale the image data into standardized space was linear and should have preserved relative brain shape while correcting for the brain size difference between groups, it is possible that the effects observed in the frontal lobe in scaled image space are an artefact of the transformation. This is because the relative size of various structures must be altered to some extent for all subjects in both groups to fit into the same size 'bounding box' (i.e. scaling). Because the parietal lobes are too small in the ALC subjects, it is possible that the frontal lobes became larger to accommodate the transformation into scaled standard space. Thus, differences in the dorsal frontal lobe may not be localizable to that region once the image data is scaled from its original size and shape. Of course, the same argument could be made for the effects observed in the parietal lobes, but converging evidence in the results from all image analyses conducted, including reduced volume, shape abnormality and tissue density abnormalities, lead to the same conclusions in the perisylvian region. There is also some evidence to corroborate the frontal effects from surface-based analyses with the more conventional volumetric data. Specifically, non-brain size corrected measures of frontal lobe volume are too small in the ALC subjects, but brain size corrected proportional measures tend to be too large. Additionally, we made *a priori* predictions that we would see frontal lobe abnormalities because neurocognitive studies in ALC subjects suggest that they are impaired in tasks of frontal lobe functioning (Mattson *et al.*, 1999). Thus, despite the ambiguity in interpreting the dorsal frontal lobe effects, whether they are too small, or spared relative to overall brain size reduction, it is not likely that the dorsal frontal lobes are functioning normally in the prenatally alcohol-exposed.

Unpredicted but highly significant decreases in DFC were observed in the orbital frontal cortex, particularly in the left hemisphere. These effects are distinct and perhaps opposite from those observed on the dorsal surface of the frontal lobes, where brain surface extent appears relatively spared. Functionally, the dorsolateral and orbital frontal lobes tend to be dissociable, where on a very simplistic level, the more dorsal regions are thought to be most responsible for planning and attention, and the more orbital regions are thought to be most responsible for inhibiting inappropriate behavior (Fuster, 1997). ALC subjects tend to be impaired on both aspects of frontal lobe functioning (Mattson *et al.*, 1999), again suggesting that both dorsal and orbital abnormalities are functionally significant in prenatal alcohol exposure.

Volumetric measures of gross lobar structures tend to be consistent with the results from surface-based analyses. That is, parietal lobe volume is highly significantly reduced in the ALC subjects, where they show evidence for the greatest decreases in DFC in the surface-based analyses. Proportional frontal lobe volume is actually too high (at trend-level significance) relative to total brain volume in the ALC subjects, where they also show evidence for increased DFC in the more dorsal regions in the scaled images. Note that the robust DFC decreases in the ventral cortex (which are no longer present in the scaled image surface analyses shown in Fig. 6) may be reflective of total frontal lobe volume reduction in the non-brain size corrected volumetric measures shown in Table 2. White matter volumes are also consistent with the surface-based analyses of gray matter density, given that regions of increased gray matter density in the statistical maps are also regions of white matter density decrease, as shown in our earlier report where voxel-based methods were used (Sowell *et al.*, 2001b). Generally, white matter volumes are too low in the ALC subjects, with the greatest decrease observed in temporal cortex followed in magnitude by decreases in parietal cortex. It is not clear why volumetric measures of gray matter do not correspond more closely with the statistical maps of gray matter density, but the results do reinforce the notion that while we measured the proportion of segmented gray matter at each surface point, by default this measure also reflects the local density of white matter and CSF.

Assessment of the volume of gray matter underlying the region of statistically significant increase in gray matter density provides some evidence that the surface- or voxel-based methods do afford higher spatial resolution in the assessment of the effects of prenatal alcohol exposure on gray matter. With the surface-based methods, we have been able to assess smaller regions that are anatomically matched across subjects, but may not have clearly definable boundaries necessary for detailed volumetric assessments. For example, in the volumetric results, the frontal lobes do not appear to be particularly affected more than any other region, but that could result from the robust decreases in brain surface extent on the ventral brain surface being 'canceled' when the relatively spared dorsal surfaces are combined in the gross frontal lobar measure studied volumetrically. Also illustrative of this point, while overall gray matter volume is reduced in the temporal lobe in the ALC subjects, these new analyses with higher spatial resolution have shown that there is a region of spared or even increased gray matter volume as well. Notably, the increased gray matter volume in the lateral posterior temporal lobes may be related to findings of spared hippocampal volume in the same subjects (Archibald *et al.*, 2001), given that anatomically the hippocampus lies just mesial to the region where we see local gray matter volume increase. The correspondence between results from more conventional, volumetric analyses and the surface-based analyses helps validate the use of more sophisticated image warping and cortical mapping algorithms in studies of abnormal brain development.

Notes

Funding support for this work was provided by: NIMH K01 MH01733

(P.I., E.R.S.); NCRR P41 RR13642, NINDS NS3753 (P.I., A.W.T.); NIAAA AA 10417 (P.I., E.P.R.); and AA 10820 (P.I., S.N.M.).

Address correspondence to: Elizabeth R. Sowell, Laboratory of Neuro Imaging, University of California, Los Angeles, 710 Westwood Plaza, Room 4-238, Los Angeles, CA 90095-1769, USA. Email: esowell@loni.ucla.edu.

References

Abel EL, Sokol RJ (1987) Incidence of fetal alcohol syndrome and economic impact of FAS-related anomalies. Drug Alcohol Depend 19:51–70.

Archibald SL, Fennema-Notestine C, Gamst A, Riley EP, Mattson SN, Jernigan TL (2001) Brain dysmorphology in individuals with severe prenatal alcohol exposure. Dev Med Child Neurol 43:148–154.

Back SA, Gan X, Li Y, Rosenberg PA, Volpe JJ (1998) Maturation-dependent vulnerability of oligodendrocytes to oxidative stress-induced death caused by glutathione depletion. J Neurosci 18: 6241–6253.

Back SA, Luo NL, Borenstein NS, Levine JM, Volpe JJ, Kinney HC (2001) Late oligodendrocyte progenitors coincide with the developmental window of vulnerability for human perinatal white matter injury. J Neurosci 21:1302–1312.

Bookstein FL, Sampson PD, Streissguth AP, Connor PD (2001) Geometric morphometrics of corpus callosum and subcortical structures in the fetal-alcohol-affected brain. Teratology 64:4–32.

Duvernoy HM, Cabanis EA, Vannson JL (1991) The human brain: surface, three-dimensional sectional anatomy and MRI. Wien: Springer.

Evans AC, Kamber M, Collins DL, MacDonald D (1994) An MRI-based probabilistic atlas of neuroanatomy. In: Magnetic resonance scanning and epilepsy (Shorvon SD, ed.), pp. 263–274. New York: Plenum.

Evans AC, Collins DL, Holmes CJ (1996) Automatic 3-D regional MRI segmentation and statistical probabilistic anatomical maps. New York: Academic Press.

Friede RL (1989) Gross and microscopic development of the central nervous system. In: Developmental neuropathology, 2nd edn (Friede RL, ed.), pp. 2–20. Berlin: Springer.

Fuster JM (1997) The prefrontal cortex: anatomy, physiology, and neuropsychology of the frontal lobe, 3rd edn. New York: Lippincott-Raven.

Guerri C (1998) Neuroanatomical and neurophysiological mechanisms involved in central nervous system dysfunctions induced by prenatal alcohol exposure. Alcohol Clin Exp Res 22:304–312.

Guerri C, Pascual M, Renau-Piqueras J (2001) Glia and fetal alcohol syndrome. Neurotoxicology 22:593–599.

Huttenlocher PR (1979) Synaptic density in human frontal cortex – developmental changes and effects of aging. Brain Res 163:195–205.

Ikonomidou C, Bittigau P, Ishimaru MJ, Wozniak DF, Koch C, Genz K, Price MT, Stefovska V, Hörster F, Tenkova T, Dikranian K, Olney JW (2000) Ethanol-induced apoptotic neurodegeneration and fetal alcohol syndrome. Science 287:1056–1060.

Ikonomidou C, Bittigau P, Koch C, Genz K, Hoerster F, Felderhoff-Mueser U, Tenkova T, Dikranian K, Olney JW (2001) Neurotransmitters and apoptosis in the developing brain. Biochem Pharmacol 62:401–405.

Jernigan TL, Ostergaard AL, Fennema-Notestine C (2001) Mesial temporal, diencephalic, and striatal contributions to deficits in single word reading, word priming, and recognition memory. J Int Neuropsychol Soc 7:63–78.

Jones KL, Smith DW (1973) Recognition of the fetal alcohol syndrome in early infancy. Lancet 2:999–1001.

Jones KL, Smith DW (1975) The fetal alcohol syndrome. Teratology 12:1–10.

MacDonald D, Avis D, Evans A (1994) Multiple surface identification and matching in magnetic resonance images. Proc Visual Biomed Comput 2359:160–169.

MacDonald D, Kabani N, Avis D, Evans AC (2000) Automated 3-D extraction of inner and outer surfaces of cerebral cortex from MRI. Neuroimage 12:340–356.

Maier SE, West JR (2001) Regional differences in cell loss associated with binge-like alcohol exposure during the first two trimesters equivalent in the rat. Alcohol 23:49–57.

Mattson SN, Riley EP (1998) A review of the neurobehavioral deficits in children with fetal alcohol syndrome or prenatal exposure to alcohol. Alcoholism Clin Exp Res 22:279–294.

Mattson SN, Riley EP (1999) Implicit and explicit memory functioning in children with heavy prenatal alcohol exposure. J Int Neuropsychol Soc 5:462–471.

Mattson SN, Riley EP, Delis DC, Stern C, Jones KL (1996) Verbal learning and memory in children with fetal alcohol syndrome. Alcoholism Clin Exp Res 20:810–816.

Mattson SN, Goodman AM, Caine C, Delis DC, Riley EP (1999) Executive functioning in children with heavy prenatal alcohol exposure. Alcoholism Clin Exp Res 23:1808–1815.

Mazziotta JC, Toga AW, Evans A, Fox P, Lancaster J (1995) A probabilistic atlas of the human brain: theory and rationale for its development. The International Consortium for Brain Mapping (ICBM). Neuroimage 2:89–101.

Miller MI, Massie AB, Ratnanather JT, Botteron KN, Csernansky JG (2000) Bayesian construction of geometrically based cortical thickness metrics. Neuroimage 12:676–687.

Olson HC, Feldman JJ, Streissguth AP, Sampson PD, Bookstein FL (1998) Neuropsychological deficits in adolescents with fetal alcohol syndrome: clinical findings. Alcoholism Clin Exp Res 22:1998–2012.

Ono, M., Kubik, S, Abernathey, C. D. (1990) Atlas of the cerebral sulci. G. Thieme Verlag; Thieme Medical Publishers, Stuttgart New York.

Roebuck TM, Mattson SN, Riley EP (1998) A review of the neuroanatomical findings in children with fetal alcohol syndrome or prenatal exposure to alcohol. Alcoholism Clin Exp Res 22:339–344.

Roebuck TM, Mattson SN, Riley EP (1999) Behavioral and psychosocial profiles of alcohol-exposed children. Alcoholism Clin Exp Res 23:1070–1076.

Sowell ER, Thompson PM, Holmes CJ, Batth R, Jernigan TL, Toga AW (1999) Localizing age-related changes in brain structure between childhood and adolescence using statistical parametric mapping. Neuroimage 9:587–597.

Sowell ER, Mattson SN, Thompson PM, Jernigan TL, Riley EP, Toga AW (2001a) Mapping callosal morphology and cognitive correlates: effects of heavy prenatal alcohol exposure. Neurology 57:235–244.

Sowell ER, Thompson PM, Mattson SN, Tessner KD, Jernigan TL, Riley EP, Toga AW (2001b) Voxel-based morphometric analyses of the brain in children and adolescents prenatally exposed to alcohol. Neuroreport 12:515–523.

Sowell ER, Thompson PM, Tessner KD, Toga AW (2001c) Mapping continued brain growth and cortical gray matter density reduction in frontal cortex: inverse relationships during post adolescent brain maturation. J Neurosci 21:8819–8829.

Sowell ER, Thompson PM, Rex D, Kornsand D, Jernigan TL, Toga AW (2002a) Mapping sulcal pattern asymmetry and local cortical surface gray matter proportion *in vivo*: maturation in posterior perisylvian cortices. Cereb Cortex 12:17–26.

Sowell ER, Trauner DA, Gamst A, Jernigan TL (2002b) Development of cortical and subcortical brain structures in childhood and adolescence: a structural magnetic resonance imaging study. Dev Med Child Neurol 44:4–16.

Swayze VW II, Johnson VP, Hanson JW, Piven J, Sato Y, Giedd JN, Mosnik D, Andreasen NC (1997) Magnetic resonance imaging of brain anomalies in fetal alcohol syndrome. Pediatrics 99:232–240.

Thompson PM, Woods RP, Mega MS, Toga AW (2000) Mathematical/computational challenges in creating deformable and probabilistic atlases of the human brain. Hum Brain Mapp 9:81–92.

Thompson PM, Mega MS, Woods RP, Zoumalan CI, Lindshield CJ, Blanton RE, Moussai J, Holmes CJ, Cummings JL, Toga AW (2001) Cortical change in Alzheimer's disease detected with a disease-specific population-based brain atlas. Cereb Cortex 11:1–16.

Woods RP, Mazziotta JC, Cherry SR (1993) MRI–PET registration with automated algorithm. J Comput Assist Tomogr 17:536–546.

Yakovlev PI, Lecours AR (1967) The myelogenetic cycles of regional maturation of the brain. In: Regional development of the brain in early life (Minkowski A, ed.), pp. 3–70. Oxford: Blackwell Scientific.

Zoeller RT, Butnariu OV, Fletcher DL, Riley EP (1994) Limited postnatal ethanol exposure permanently alters the expression of mRNAS encoding myelin basic protein and myelin-associated glycoprotein in cerebellum. Alcohol Clin Exp Res 18:909–916.